Flexural strength of 3Y-TZP bioceramics obtained by Direct Write Assembly as function of residual connected-porosity

Joana Baltazar[1,2], Manuel Fellipe Rodrigues Pais Alves[1], Manuel A, Martins [1], Paula M.C Torres[1], Claudinei Santos[3]*, Susana Olhero[1]

[1] *Department of Materials and Ceramic Engineering, CICECO - Aveiro Institute of Materials, University of Aveiro, Aveiro, Portugal*
[2]*Department of Mechanical Engineering, TEMA- Centre for Mechanical Technology and Automation, University of Aveiro, Portugal*
[3] *Materials and Processes Laboratory, Faculty of Technology, Rio de Janeiro State University, FAT-LMP/UERJ, Resende - RJ, Brazil*

Abstract

The present work reports the effect of the extrusion nozzles' size and consequent residual porosity on the flexural strength of 3Y-TZP bioceramics fabricated by direct write assembly technology. A printable ink containing a volume fraction of 45 % of 3Y-TZP (ZrO_2 stabilized with 3 mol% Y_2O_3) submicron powder, carboxymethyl cellulose and polyethyleneimine as additives was fine-tuned by rheological measurements. Different nozzle diameters (0.41 mm, 0.33 mm, and 0.25 mm) were used to print 3D specimens with proper dimensions for structural and mechanical characterization after sintering, namely relative density, linear shrinkage, and three-point flexural strength. Bulk surface sample and exposed fractured surfaces after flexural strength tests were analyzed by X-ray diffraction, Rietveld refinement and scanning electronic microscopy. Strength reliability and failure probability of the three sample groups were analyzed by Weibull statistics.

The sintered samples exhibited relative densities in the range of 78 % (nozzle Ø 0.41 = mm) and 82 % (nozzle Ø 0.25 = mm), i.e., a slight increase in the residual interfilamentous porosity is observed, as the extrusion tip diameter increases, while linear shrinkage is statistically similar (≈ 25 %). Likewise, a progressive reduction of flexural strength and Weibull modulus as nozzle diameter increases was noticeable, being respectively σ_f = 337,5 ± 49 MPa and m = 6.6 for the smallest nozzle diameter (Ø = 0.25 mm) and σ_f = 261.4 ± 79 MPa and m = 3.2 for the biggest one (Ø = 0.41 mm). Unlike nozzle diameter, the material is constituted by 79-81 wt% tetragonal *t*-ZrO_2 and 19-21 wt% cubic *c*-ZrO_2 with equiaxed grain sizes between 0.3 and 0.6 μm. X-ray diffraction analyses on the fracture surface of flexural test samples suggests that the toughening mechanism by *tetragonal→ monoclinic* phase transformation is the main responsible for the mechanical strength of this structural ceramic. Additionally, the reduction of flexural strength for samples printed with extrusion nozzle of 0.41 mm could be explained by the surface roughness of the bending surfaces, as well as the lower effective resistance to crack-propagation arising from the higher size of residual pores on the fracture surface.

Keywords: Robocasting, 3Y-TZP bioceramics, flexural strength, porosity, toughening mechanisms.
Corresponding author: claudineisvr@gmail.com

1. Introduction

Robocasting, also known as direct write assembly (DWA), is an additive manufacturing technique in which a filament ink-like material is extruded from a nozzle, layer by layer (Lewis et al., 2006; Peng et al., 2018b). This technique has been highly explored in the manufacturing of porous bioceramics-based 3D structures for tissue engineering applications (known as scaffolds), where higher specific surface area and apparent porosity are required to optimize the biological response between the material and the native tissues (Brazete et al., 2019; Daguano et al., 2007). Oppositely, the fabrication of high dense functional ceramics by this technology is not at the same research level, since the porosity generated between adjacent circular filaments is still difficult to control and eliminate. Rheological properties of the inks and printing parameters such as, in-fill patterning, printing speed and nozzle diameters are examples of potential aspects that can be fine-tuned to attain high dense ceramics by extrusion-based technologies (Baltazar et al., 2021a; Peng et al., 2018b; Rodrigues et al., 2020). Ink´s rheology is highly determined by the amounts of ceramic particles and quantity of additives as thickening agents. Increasing solids loading as much as possible and decreasing organic additives have been the main goals, since it reduces shrinkage and cracks in printed ceramic parts, enhancing density and consequently mechanical performance (Xia and Duan, 2021). Post-processing steps as drying, binder burnout and sintering can also be pointed out as important stages to control final density and mechanical performance (Rodrigues et al., 2020; Xia and Duan, 2021).

Zirconium dioxide (ZrO_2) fabrication by robocasting has already been explored in literature, due to its high applicability in dentistry (Branco et al., 2020; Galante et al., 2019; Rodrigues et al., 2020). This is a bioinert material that presents high sinterability when compared to other oxide ceramics, and a particular toughening mechanism by phase transformation, which occurs when ZrO_2 presents itself in the metastable tetragonal phase obtained from its stabilization with different oxides such as Y_2O_3, CeO_2 or MgO (Chevalier et al., 2009; Deville et al., 2004). Yttrium stabilized zirconia (Y-TZP) is one of the most popular alternatives because it presents high flexural strength and fracture toughness superior to other oxides. Due to these characteristics, Y-TZP has been widely used in the subtractive manufacture of dental prostheses by CAD/CAM (Computer Aided Design/Computer Aided Manufacturing), milling and injection molding technique (Denry and Kelly, 2008; Miyazaki et al., 2013).

Regarding fabrication of this particular material by robocasting, the development of printable inks to attain high dense structures has been the main focus in previous works (Balani et al., 2021; Mohammadi et al., 2021; Özkol et al., 2012; Peng et al., 2018a). Insufficient density and lack of mechanical properties are the main problems, being still scarce the literature works that tried to face

these difficulties in zirconia-based ceramics (Mohammadi et al., 2021; Peng et al., 2018a; Rodrigues et al., 2020; Zhao et al., 2021). For example, Peng et al. (Peng et al., 2018a) stated the use of robocasting to attain porous and dense yttrium stabilized zirconia structures from inks containing up to 38 vol% solids loading. Even if the optimization of the rheological properties of the ink and sintering step allowed to obtain highly dense structures (97.8 %), flexural strength was not higher than 243 MPa. Recently, Xiaoguang Xia and Guolin Duan (Xia and Duan, 2021) reported the advantages of inks containing high solids loading (58 vol%) to attain dense zirconia structures (98.8 % relative density) and high flexural strength (3 point flexural strength test) values (676 ± 10 MPa) for grounded samples with 55 mm × 7 mm × 2.5 mm measurements sintered at 1550 ºC for 2 h . However, besides properties of the inks, the nozzle size used in the extrusion process and the inherent filament diameter can strongly affect the surface quality of the printed parts, as well as the final structural performance. From the authors' knowledge this is a topic not yet explored in literature for zirconia-based fabrication by direct write assembly.

In this way, the present work discusses the effect of printing nozzle' sizes in the resultant internal porosity between filaments and consequently, on the structural performance of final zirconia printed parts by robocasting. 3Y-TZP samples printed with three different nozzle sizes were produced and characterized by density, flexural strength, microstructure, and phases formed, demonstrating the limitations of this printing parameter in zirconia ceramics with future potential applications in dentistry, such as dental prostheses.

2. Experimental Procedure

2.1. Inks preparation and characterization

A commercial zirconia powder stabilized with 3 mol% of yttrium oxide, 3Y-TZP, (TZ-3YS TOSOH-Corp., Japan), with a specific surface area of 6.7 m^2g^{-1} was used in this study. A colloidal suspension containing a total of 45 vol% of solids was firstly prepared by dispersing the powder in deionized water in presence of 1 wt% (based on solids amount) Dolapix CE64 (Zimmer and Schwartz, Germany). The suspension was deagglomerated in a ball milling with zirconia spheres for 24 h. Then, the suspension was thickened by adding 0.2 wt% (based on 3Y-TZP solids amount) of carboxymethyl cellulose (CMC, 250 000 Mw, Colorobia, Portugal) and the mixture homogenized in a planetary centrifugal mixer (ARE-250, Thinky Co., Tokyo, Japan) during 10 min at 800 rpm. Finally, different amounts of polyethyleneimine solution (PEI, Sigma-Aldrich, USA, Mn ~1800 and Mw ~2000), namely 0.05, 0.1, 0.2 and 0.25 wt% (based on 3Y-TZP solids amount), were added to fine-tune extrudable inks with adequate stiffness for extrusion-based 3D printing. The final ink was mixed and

degassed using again the planetary centrifugal mixer during 5 min at 1000 rpm to guarantee high homogeneity. The suspension and the respective inks were characterized at room temperature (25 ºC) by rheological properties using a rotational rheometer (Kinexus Pro^{+}, Malvern, UK), holding a solvent trap to prevent samples drying during experiments. The shear viscosity was measured using a cone/plate system (4º/40 mm) with a gap of 150 µm in the shear rate range of 0.1 to 1000 s^{-1}. Viscoelastic properties of the inks were evaluated by amplitude sweep measurements at 1 Hz frequency in oscillatory mode, using a plate sensor (Φ = 20 mm), with 1 mm gap size.

2.2. Robocasting process

A robocasting system (Model EBRD-A32, 3D Inks, LLC, USA) was used to print prismatic zirconia structures with the as-prepared ink as feedstock material. The ink was loaded into a 5 mL syringe (Nordson, USA) and extruded through a nozzle with different diameters (0.25, 0.33 and 0.41 mm) with 10 mm/s printing speed. The zirconia structures were constructed on a smooth alumina plate at room temperature with controlled humidity (~85 % relative humidity, RH). After printing the zirconia samples were gradually dried at room temperature with controlled humidity for 24 h to avoid bending. In-fill patterning orientation previously demonstrated as resulting in better mechanical properties was selected (Baltazar et al., 2021b) and the 3D-models designed in RoboCAD software, varying the filament dimensions. Green dimensions of approximately 57 x 5.5 x 4.7 mm (length x height x width) were used in CAD models to respect standardized testing structures after sintering for mechanical properties. **Figure 1** shows the CAD model of the three green configurations and the details of the cross section used in the fabrication of the rectangular samples. After drying for 24 h, the samples were inspected and those with bending superior to 5 % were discarded, as exemplified in **Figure 2**.

Figure 1

Figure 2

2.3. Sintering and characterization of 3Y-TZP printed samples

A minimum of 10 samples (n >10 bars/group) printed with each nozzle diameter were obtained for subsequent characterization. After printing and drying steps, the ceramic structures were sintered at 1550 °C using the schedule presented in **Figure 3**.

Figure 3

Linear shrinkage was measured from dried to sintered samples. Bulk density of all sintered structures was measured by Archimedes immersion method according to ASTM C20-00 (Astm C20, 2017). For that, samples were dried at 110 ºC until achieving a constant mass in 3 consecutive measurements (D). The dried samples were then placed in water and boiled for 2 h, avoiding the contact with the heated bottom part of the container and kept immersed in water for 12 h. After saturation, the mass of the samples was determined while they were submerged in water (S). Then, the samples were lightly rolled on a wet cloth to remove the excess of superficial water and weighted to determine its water-saturated weight (W). The bulk density was determined according to Equation (1).

$$\rho = D/[(W - S)/\rho_{water}\,] \qquad (1)$$

where: ρ is the bulk density; D is the dry mass; W is the mass of water-saturated sample, S is the mass of the sample submerged in water and ρ_{water} is the water density. The mechanical strength of the sintered bars was evaluated by three-point flexural test in a universal testing machine (AG-IS 10kN, Shimadzu Corpor., Kyoto, Japan) according to the ASTM C1161-18 standard (International, 1996). Tests were carried out in the perpendicular direction to the printing plane of the 3D bars at constant speed of 0.5 $mm.min^{-1}$. The original printing surfaces of the zirconia samples were kept for the performance of the three-point bending tests. These results were statistically analyzed using Weibull statistics according to procedures detailed in previous works (Quinn and Quinn, 2010).

Qualitative and quantitative crystalline phase analyses on the surface sintered samples and on the fracture surface after 3-point flexural testing, to evaluate phase transformations that occurred in this region, were obtained by combining x-ray diffraction (XRD) and Rietvelt refinement. A high resolution X'Pert PRO diffractometer (Malvern PANanalytical, Worcestershire, United Kingdom) was used to record XRD data within the 2θ range of 20°- 80° with a step size 0.02° and 100 s of counting time for each step. The FullProf software was used for Rietveld refinement. Morphological and microstructural analyses of the 3Y-TZP printed samples with the different nozzle diameters (surface and cross-section in fracture surfaces after flexural tests) were evaluated by optical microscopy and scanning electron microscopy (SEM, Hitachi S4100, Hitachi High-Technologies Europe, GmbH, Germany) and subsequently analyzed using *IMAGE J* software.

3. Results and discussion

3.1. Inks characterization

Robocasting technique needs a strict control on the rheological properties of the inks to attain good printing behavior and consequently, printed parts with the required geometry. An ink suitable for this technique should hold proper viscoelastic characteristics to allow simultaneously an easy flow through a tight nozzle and a shape retention of the filament immediately after printing. Moreover, printed filaments should have sufficient mechanical strength to support the weight of the subsequent layers (Baltazar et al., 2021b; Gaddam et al., 2021). **Figure 4 (a)** illustrates the effect of different concentrations of PEI in the loss (G'') and storage (G') modulus of the inks as function of shear stress, when compared with the suspension only in presence of CMC. This study was evaluated in oscillatory mode instead of viscometry since flow curves involve extensive deformations that destroy the internal structure of the systems. **Figure 4 (b)** presents the viscosity *versus* shear rate curves of the 3Y-TZP suspensions and respective inks in presence of the selected amounts of additives (CMC or CMC+PEI) to evaluate the flow behavior of the final systems.

Figure 4

The ink containing only CMC presents a linear viscoelastic region plateau up to about 7-8 Pa, where further increase in the shear stress values leads to a collapse of their internal structure, meaning that this system will not present enough mechanical stability during printing. Furthermore, it is known from literature that a storage modulus (G') higher than 10^4 Pa is required to attain printable inks for robocasting. This is not acquired when just CMC is added to the suspension (Baltazar et al., 2021b; Nan et al., 2019; Rodrigues et al., 2020) that plays a role of thickening agent. The addition of PEI promotes the increase of the elastic modulus, transforming the viscous-like suspensions into solid-like inks, with G' in the range of 10^6-10^7 Pa. In fact, the addition of PEI promotes the coagulation effect as mentioned in other reports (Baltazar et al., 2021b; Gaddam et al., 2021; Marques et al., 2017), explained by the interaction of the cationic secondary and tertiary amino groups from PEI with negatively charge functional groups of dispersant adsorbed at zirconia particles (Dolapix CE64), inhibiting the charges, and consequently promoting particles' agglomeration. Regardless the PEI amount, all inks stay stable over a wide range of applied shear stress values (at least until 100 Pa), indicating that the filaments will be mechanically stable during the printing process with sufficient strength to support the weight of consecutive layers (Baltazar et al., 2021b; Gaddam et al., 2021; Marques et al., 2017; Nan et al., 2019). The rupture of the network formed between the polymeric

matrix and the 3Y-TZP particles (yield stress point) is noticeable when G'' intersect the G', i.e., there is a transition from a solid-like to a liquid-like system. As the amount of PEI increases, this transition occurs at higher applied shear stress, indicating that a stronger gel is formed (Baltazar et al., 2021b; Gaddam et al., 2021; M'Barki et al., 2017). Given the similar behavior observed for 0.2 wt% and 0.25 wt% of PEI and having in mind the importance of using lower amounts of organic additives, 0.2 wt% of PEI was the amount selected for the final printable inks. Comparing the flow behavior (**Figure 4 (b)**) of the 3Y-TZP colloidal suspensions containing 45 vol% of solids in absence and in presence of CMC, as well as the final ink comprising CMC and PEI, it's possible to observe that all systems exhibit shear-thinning behavior, where the viscosity decreases as shear rate increases, indicating that this solid loading and amounts of additives are suitable to go ahead with printing process. As expected, the viscosity of the base suspension increases with the addition of the additives, highly pronounced when PEI is added.

3.2. Structural properties of 3Y-TZP samples

Figure 5 presents results of relative density, linear shrinkage, X-Ray diffraction and SEM micrographs of the 3Y-TZP samples printed by robocasting. Crystalline phases and microstructure were not dependent on the extrusion-nozzle diameter, being the results presented in this Figure demonstrative of the sintered 3Y-TZP bulk material.

Figure 5

As it can be seen, after sintering the linear shrinkage was in the range of 24.8 % - 24.9 %, without considerable statistical variations among the different groups, while the relative density displayed a slight variation depending on the nozzle diameter used during the extrusion process. In fact, for the green samples, the results should be consistent with the filament overlap configuration presented in **Figure 2**, and this Figure displays that the voids between layers and adjacent filaments are higher in structures printed with a nozzle diameter of 0.410 mm (RZ-410) when compared to the smaller ones (RZ-330 and RZ-250). Moreover, the sintering cycle adopted in this work (**Figure 3**), considers a slow heating rate to facilitate binders' removal and a usual sintering temperature for zirconia-based ceramics (1550 ºC), aiming to improve the densification of the samples and preventing the overgrowth of the ZrO_2 grains (Palmeira et al., 2016). Even considering these adopted sintering conditions, a residual porosity around 20 % is still present in the dimensional structure of all sintered ceramic samples, located preferentially in the critical points between filaments, denoting that sintering and densification mechanisms were not effective in its elimination. Decreasing the tip

diameter (RZ-250), a slight reduction in porosity is observed, leading to an average relative density in the final ceramic structure of approximately 82 %. Concerning crystalline phases composition of the sintered ceramics, a mixture of tetragonal *t*-ZrO_2 (80 ± 1 %) and cubic *c*-ZrO_2 (20 ± 1 %) phases is noticeable from X-ray diffraction results and Rietveld refinement as presented **Figure 5 (b)**, in good agreement with other recent reports related to 3Y-TZP ceramics (Basu, 2005; Chevalier et al., 2009; Hannink et al., 2000). The original surface microstructure of the 3Y-TZP sintered samples at 1550 ºC for 2 h is shown in **Figure 5 (c)**. The ZrO_2 grains present equiaxial morphology with submicron sizes in the range of 0.3 μm and 0.6 μm. The nonappearance of abnormal grain growth is a good indication that the attained microstructure offers high potential for toughening, in accordance with previous reports that stated a preferential grain-size range (0.1 to 1.0 μm) to enhance toughening mechanisms by *tetragonal→monoclininc (t→m)* phase transformation (Basu, 2005; Garvie and Goss, 1986).

Figure 6 (a) and **(b)** presents the results of Weibull statistics and probability of fracture (pf) as function of flexural strength of sintered 3Y-TZP samples obtained with the three different nozzles. Mean flexural strength values of 261.4 ± 79 MPa, 288.8 ± 57 MPa and 337.5 ± 47 MPa were obtained respectively for RZ-410, RZ-330 and RZ-250. Thus, an inverse ratio between the extrusion nozzle diameter and flexural strength was demonstrated, i.e., flexural strength increases as nozzle diameter used in the 3D-printing process decreases. Likewise, the Weibull modulus obtained by statistical analysis of the different groups was m= 3.2, m= 4.4 and m= 6.6, for RZ- 410, RZ- 330 and RZ- 250 groups, respectively. This flexural strength values are somewhat inferior when compared to the results attained by Xia and Duan, 2021 (676 ± 10 MPa) for the same material using a tip diameter of 0.5 mm. The additives used by the authors and rheological properties attained could be the reason for these differences. While in the present work the final inks presented elastic modulus (G') in the order of 10^6-10^7 Pa, the G' values for the high solid loaded inks (58 vol%) in Xia and Duan 2021 work are lower (between 1000 and 10000 Pa), meaning that ink could slightly deformed after printing and fill the inter-filament gaps. This approach was avoided in this work, since the aim was to evaluate the influence of inter-filament porosity in the flexural strength of printed samples.

The three-point flexural strength test presents typical features related with geometric configuration, namely a stress distribution with maximum peaks located in the center of the samples where the load is applied, as illustrated in **Figure 6 (c)**. In the present work, the surface of the samples after printing was maintained (no polishing applied), to identify possible influences of the surface finishing resolution, resultant to the different nozzle sizes, in the flexural performance. In this context, **Figure**

7 presents the profiles of these surfaces, corresponding to the tensile surface of the samples during the flexural strength test.

Figure 6
Figure 7

As it can be seen from **Figure 7**, surface roughness increases as filament diameter increases, as expected, with the more sinuous topographies (indicating higher roughness) observable for the samples extruded with 0.41 mm nozzles (RZ-410). The larger space between filaments with higher diameters explains this phenomenon and proves that surface integrity of the samples remains stable after the sintering process, according to the results previewed by the rheological measurements of the inks. Additionally, **Figure 8** and **Figure 9** presents X-ray diffraction and SEM micrographs, respectively, of the 3Y-TZP samples' fracture surface (RZ-410, RZ-330 and RZ-250) after bending tests.

Figure 8
Figure 9

The results presented in **Figure 8** demonstrated that the tetragonal ZrO_2 grains adjacent to the fracture surface exhibit a typical martensitic transformation to a monoclinic phase (*m*-ZrO_2), being a phase transformation mechanism well known and discussed in previous works (Basu, 2005; Chevalier et al., 2009). During the propagation of a failure, such as flexural fracture, the grains are subjected to external stresses that exceed the strain required for the *tetragonal* to *monoclinic* transformation to occur. Consequently, the grains in the periphery of this new fracture surface are converted into a monoclinic ZrO_2 phase that can be detected by X-ray diffraction. In the diffractograms shown in **Figure 8**, the transformed monoclinic phase content is in the order of 17 % - 19 %, regardless the size of the extrusion nozzle used.

Observing the fracture profile in SEM micrographs (**Figure 9**), symmetric and organized residual pores are evident, even after sintering, representative of the voids created from the deposited filaments, according to the scheme represented in **Figure 2**. The two-dimensional analysis of SEM micrographs with low magnification (100x) from Figure 9, revealed the porosity profile in each studied group (RZ-250, RZ-330 and RZ-410). An increase in total porosity as a function of the printing nozzle was observed for standardized areas of 1275 x 900 μm, going from 4.6 % planar porosity (RZ-250) to 6.3 % (RZ-410). Therefore, in addition to the lower total porosity noticeable in

zirconia printed with a 0.250 mm tip (RZ-250), a reduction in the average pore size was identified when compared to 3Y-TZP samples printed with larger nozzles. Higher magnifications of the SEM micrographs for the different sample groups (RZ-250, RZ-330 and RZ-410) demonstrated that the microstructure (equiaxial grains of ZrO_2) in the inner filament of the cross section is similar for all configurations studied, in good agreement with results obtained for the original surface of the printed samples (**Figure 5(c)**). These results were somewhat expected, since all samples were sintered with the same sintering schedule.

The reported flexural strength values for 3Y-TZP ceramics, sintered in similar temperature range, are typically in the order of 800 - 900 MPa, when relative density is higher than > 97% (Amarante et al., 2019; Shelar et al., 2021). The outcomes attained in the present work (flexural strength in the range of 260-350 MPa), using robocasting as processing method, are still far away from those values, highly related to the presence of residual connected porosity that gives rise to final ceramics with low densification (between 79 % and 82 %). Additionally, the original tensile surface of the samples, containing irregularities typical of an extrusion-based printing process from filaments, can be highlighted as the main reason for the flexural strength differences observed in the 3Y-TZP samples with different nozzle sizes, RZ- 410, RZ- 330, and RZ- 250. In fact, the topography of each processing condition indicated that the surface roughness may interfere with the final values of flexural strength, in agreement with a previous literature report (Shelar et al., 2021), where authors verified that roughness parameters presented in the surface region of the test flexural samples reduce considerably the bending strength of 3Y-TZP ceramics. Furthermore, as the applied stress reaches values that allow crack propagation, smaller volumes of tetragonal ZrO_2 grains are expected in the fracture region of the RZ-410 group samples during its propagation (as can be confirmed in **Figure 8**), since the residual connected porosity in this group is larger than RZ-330 and RZ-250 (Figures 2 and 5). Thus, less resistance to crack propagation is expected in these RZ-410 ceramics, resulting in less flexural strength.

The flexural performance of 3Y-TZP ceramics fabricated by an additive manufacturing technology as robocasting is of particular interest, having ahead its use in dental applications such as prostheses. According to ISO 6872-15 "Dental ceramics" (“ISO - ISO 6872:2015 - Dentistry — Ceramic materials,” n.d.), one of the main mechanical requirements for dental applications is the flexural strength. According to this standard, different demands in flexural strength are needed, according to the dentistry application as demonstrated in **Figure 10**. For example, "Monolithic ceramic for three-unit prostheses involving molar restoration" or "Partially or fully covered substructure for three-unit prostheses involving molar restoration” belongs to Group 4 (G4, minimum binding strength 500

MPa), while "Monolithic ceramic for prostheses involving partially or fully covered substructure for four or more units or fully covered" or even "Substructure for prostheses involving four or more units" demands higher mechanical performance (Group 5, G5), requiring a minimum strength of 800 MPa.

Figure 10

On the other hand, other applications, such as "Monolithic ceramic for single-unit anterior or posterior prostheses and for three-unit prostheses not involving molar restoration adhesively or non-adhesively cemented" from Group 3 (G3) required less flexural strength parameters (> 300 MPa), or even others less demanding such as Group 1 (G1) and group 2 (G2), superior to 50 or 100 MPa, respectively. According to this, Direct Writing Assembly (DWA) technique to manufacture 3Y-TZP anatomical parts for dentistry field presents high potential, although future efforts are needed to improve the surface quality of printed samples and eliminate as much as possible the connected porosity between filaments.

Conclusions

Printable inks by robocasting were successfully prepared, containing 45 vol.% of commercial 3Y-TZP ceramic particles and, as thickening and coagulating agents, CMC and PEI, respectively. Keeping the rheological properties of the inks, the use of different extrusion nozzles (0.41 mm, 0.33 mm and 0.25 mm) demonstrated that smaller diameters lead to an increase in the packing degree of the printed layers, decreasing the residual connected interfilamentous porosity, as well as the superficial roughness of the samples after sintering step. A flexural strength around 350 MPa was reached by using a diameter extrusion nozzle of 0.25 mm (RZ-250). Even if still far from the typical flexural strength values usually obtained for this material, enough performance was attained to make the material mechanically viable for dental prostheses, considering robocasting as a future potential fabrication technique.

To go ahead with upcoming success in fabrication of dense zirconia parts by robocasting is of paramount importance to find a good compromise between rheological properties of the inks and printing parameters.

Acknowledgments

This work was supported by the project "TAMAZ3D - Development of a Decision Support Tool for Additive Manufacturing of Alumina-Zirconia 3-D structures" with references POCI-01-0145-FEDER-030493 and PTDC/EME-EME/30493/2017. The support by the projects of CICECO (UIDB/50011/2020 & UIDP/50011/2020) and TEMA (UID/EMS/00481/2020) financed by national funds through the FCT/MEC and when appropriate co-financed by the European Regional Development Fund (ERDF) under the PT2020 Partnership Agreement, was also acknowledged. P. M. C. Torres and S. M. Olhero acknowledge Portuguese Foundation for Science and Technology (FCT) for CEECIND/01891/2017 and CEECIND/03393/2017 contracts, respectively. C. Santos is thankful for financial support received from Brazilian agencies, FAPERJ (Grants E-26-201.476/2014 and E26-202.997/2017) and CNPq (Grant 311.119/2017-4).

References

Amarante, J.E.V., Pereira, M.V.S., de Souza, G.M., Pais Alves, M.F.R., Simba, B.G., dos Santos, C., 2019. Roughness and its effects on flexural strength of dental yttria-stabilized zirconia ceramics. Mater. Sci. Eng. A 739, 149–157. https://doi.org/10.1016/j.msea.2018.10.027

Astm C20, 2017. Standard Test Methods for Apparent Porosity, Water Absorption, Apparent Specific Gravity, and Bulk Density of Burned Refractory Brick and Shapes by Boiling Water 1 This international standard was developed in accordance with internationally recognized pri. ASTM Int. 00, 20–22. https://doi.org/10.1520/C0020-00R10

Balani, S.B., Ghaffar, S.H., Chougan, M., Pei, E., Şahin, E., 2021. Processes and materials used for direct writing technologies: A review. Results Eng. 11. https://doi.org/10.1016/j.rineng.2021.100257

Baltazar, J., Torres, P.M.C., Dias-de-Oliveira, J., Pinho-da-Cruz, J., Gouveia, S., Olhero, S., 2021a. Influence of filament patterning in structural properties of dense alumina ceramics printed by robocasting. J. Manuf. Process. 68, 569–582. https://doi.org/10.1016/j.jmapro.2021.05.043

Baltazar, J., Torres, P.M.C., Dias-de-Olveira, J., Pinho-da-Cruz, J., Gouveia, S., Olhero, S., 2021b. Influence of filament patterning in structural properties of dense alumina ceramics printed by robocasting. J. Manuf. Process.

Basu, B., 2005. Toughening of yttria-stabilised tetragonal zirconia ceramics. Int. Mater. Rev. 50, 239–256. https://doi.org/10.1179/174328005X41113

Branco, A.C., Silva, R., Santos, T., Jorge, H., Rodrigues, A.R., Fernandes, R., Bandarra, S., Barahona, I., Matos, A.P.A., Lorenz, K., Polido, M., Colaço, R., Serro, A.P., Figueiredo-Pina, C.G., 2020. Suitability of 3D printed pieces of nanocrystalline zirconia for dental applications. Dent. Mater. 36, 442–455. https://doi.org/10.1016/j.dental.2020.01.006

Brazete, D., Neto, A.S., Ferreira, J.M.F., 2019. Optimization of zirconia inks to fabricate 3D porous scaffolds by robocasting. Lek. a Tech. 49, 5–10. https://doi.org/10.14311/CTJ.2019.1.

Chevalier, J., Gremillard, L., Virkar, A. V., Clarke, D.R., 2009. The tetragonal-monoclinic transformation in zirconia: Lessons learned and future trends. J. Am. Ceram. Soc. 92, 1901–1920. https://doi.org/10.1111/j.1551-2916.2009.03278.x

Daguano, J.K.M.F., Santos, C., Souza, R.C., Balestra, R.M., Strecker, K., Elias, C.N., 2007. Properties of ZrO2-Al2O3 composite as a function of isothermal holding time. Int. J. Refract. Met. Hard Mater. 25, 374–379. https://doi.org/10.1016/j.ijrmhm.2006.12.005

Denry, I., Kelly, J.R., 2008. State of the art of zirconia for dental applications. Dent. Mater. 24, 299–307. https://doi.org/10.1016/j.dental.2007.05.007

Deville, S., Guénin, G., Chevalier, J., 2004. Martensitic transformation in zirconia Part I. Nanometer scale prediction and measurement of transformation induced relief. Acta Mater. 52, 5697–5707. https://doi.org/10.1016/j.actamat.2004.08.034

Gaddam, A., Brazete, D.S., Neto, A.S., Nan, B., Ferreira, J.M.F., 2021. Three-dimensional printing of zirconia scaffolds for load bearing applications: Study of the optimal fabrication conditions. J. Am. Ceram. Soc. 104, 4368–4380. https://doi.org/10.1111/jace.17874

Galante, R., Figueiredo-Pina, C.G., Serro, A.P., 2019. Additive manufacturing of ceramics for dental applications: A review. Dent. Mater. https://doi.org/10.1016/j.dental.2019.02.026

Garvie, R.C., Goss, M.F., 1986. Intrinsic size dependence of the phase transformation temperature in zirconia microcrystals. J. Mater. Sci. 21, 1253–1257. https://doi.org/10.1007/BF00553259

Hannink, R.H.J., Kelly, P.M., Muddle, B.C., 2000. Transformation toughening in zirconia-containing ceramics. J. Am. Ceram. Soc. 83, 461–487. https://doi.org/10.1111/j.1151-2916.2000.tb01221.x

International, A., 1996. Standard Test Method for Flexural Strength of Advanced Ceramics at Ambient. Order A J. Theory Ordered Sets Its Appl. https://doi.org/10.1520/C1161-02CR08E01.2

ISO - ISO 6872:2015 - Dentistry — Ceramic materials [WWW Document], n.d. URL https://www.iso.org/standard/59936.html (accessed 10.19.21).

Lewis, J.A., Smay, J.E., Stuecker, J., Cesarano, J., 2006. Direct ink writing of three-dimensional ceramic structures. J. Am. Ceram. Soc. 89, 3599–3609. https://doi.org/10.1111/j.1551-2916.2006.01382.x

M'Barki, A., Bocquet, L., Stevenson, A., 2017. Linking Rheology and Printability for Dense and Strong Ceramics by Direct Ink Writing. Sci. Rep. 7, 1–10. https://doi.org/10.1038/s41598-017-06115-0

Marques, C.F., Perera, F.H., Marote, A., Ferreira, S., Vieira, S.I., Olhero, S., Miranda, P., Ferreira, J.M.F., 2017. Biphasic calcium phosphate scaffolds fabricated by direct write assembly: Mechanical, anti-microbial and osteoblastic properties. J. Eur. Ceram. Soc. 37, 359–368. https://doi.org/10.1016/j.jeurceramsoc.2016.08.018

Miyazaki, T., Nakamura, T., Matsumura, H., Ban, S., Kobayashi, T., 2013. Current status of zirconia restoration. J. Prosthodont. Res. 57, 236–261. https://doi.org/10.1016/j.jpor.2013.09.001

Mohammadi, M., Becker, G., Diener, S., Tulliani, J.-M., Katsikis, N., Palmero, P., 2021. Robocasting of dense zirconia parts using commercial yttria-stabilized zirconia granules and ultrafine particles. Paste preparation, printing, mechanical properties. Ceram. Int. https://doi.org/10.1016/j.ceramint.2021.09.278

Nan, B., Olhero, S., Pinho, R., Vilarinho, P.M., Button, T.W., Ferreira, J.M.F., 2019. Direct ink writing of macroporous lead-free piezoelectric Ba 0.85 Ca 0.15 Zr 0.1 Ti 0.9 O 3. J. Am. Ceram. Soc. 102, 3191–3203. https://doi.org/10.1111/jace.16220

Özkol, E., Zhang, W., Ebert, J., Telle, R., 2012. Potentials of the " Direct inkjet printing" method for manufacturing 3Y-TZP based dental restorations. J. Eur. Ceram. Soc. 32, 2193–2201. https://doi.org/10.1016/j.jeurceramsoc.2012.03.006

Palmeira, A.A., Bondioli, M.J., Strecker, K., Santos, C. Dos, 2016. Densification and grain growth of nano- and micro-sized Y-TZP powders. Ceram. Int. 42, 2662–2669. https://doi.org/10.1016/j.ceramint.2015.10.073

Peng, E., Wei, X., Garbe, U., Yu, D., Edouard, B., Liu, A., Ding, J., 2018a. Robocasting of dense yttria-stabilized zirconia structures. J. Mater. Sci. 53, 247–273. https://doi.org/10.1007/s10853-017-1491-x

Peng, E., Zhang, D., Ding, J., 2018b. Ceramic Robocasting: Recent Achievements, Potential, and Future Developments. Adv. Mater. 30, 1–14. https://doi.org/10.1002/adma.201802404

Quinn, J.B., Quinn, G.D., 2010. A practical and systematic review of Weibull statistics for reporting strengths of dental materials. Dent. Mater. 26, 135–147. https://doi.org/10.1016/j.dental.2009.09.006

Rodrigues, I., Guedes, M., Olhero, S., Chefdor, A., Branco, A.C., Leite, M., Serro, A.P., Figueiredo-Pina, C.G., 2020. Development of free binder zirconia-based pastes for the production of dental pieces by robocasting. J. Manuf. Process. 57, 1–9. https://doi.org/10.1016/j.jmapro.2020.06.015

Shelar, P., Butler, S., Abdolvand, H., 2021. On the behaviour of zirconia-based dental materials: A review. J. Mech. Behav. Biomed. Mater. 124, 104861. https://doi.org/10.1016/j.jmbbm.2021.104861

Xia, X., Duan, G., 2021. Effect of solid loading on properties of zirconia ceramic by direct ink writing. Mater. Res. Express 8. https://doi.org/10.1088/2053-1591/abd866

Zhao, Y., Li, P., Dong, P., Zeng, Y., Chen, J., 2021. Investigation on 3D printing ZrO2 implant abutment and its fatigue performance simulation. Ceram. Int. 47, 1053–1062. https://doi.org/10.1016/j.ceramint.2020.08.221

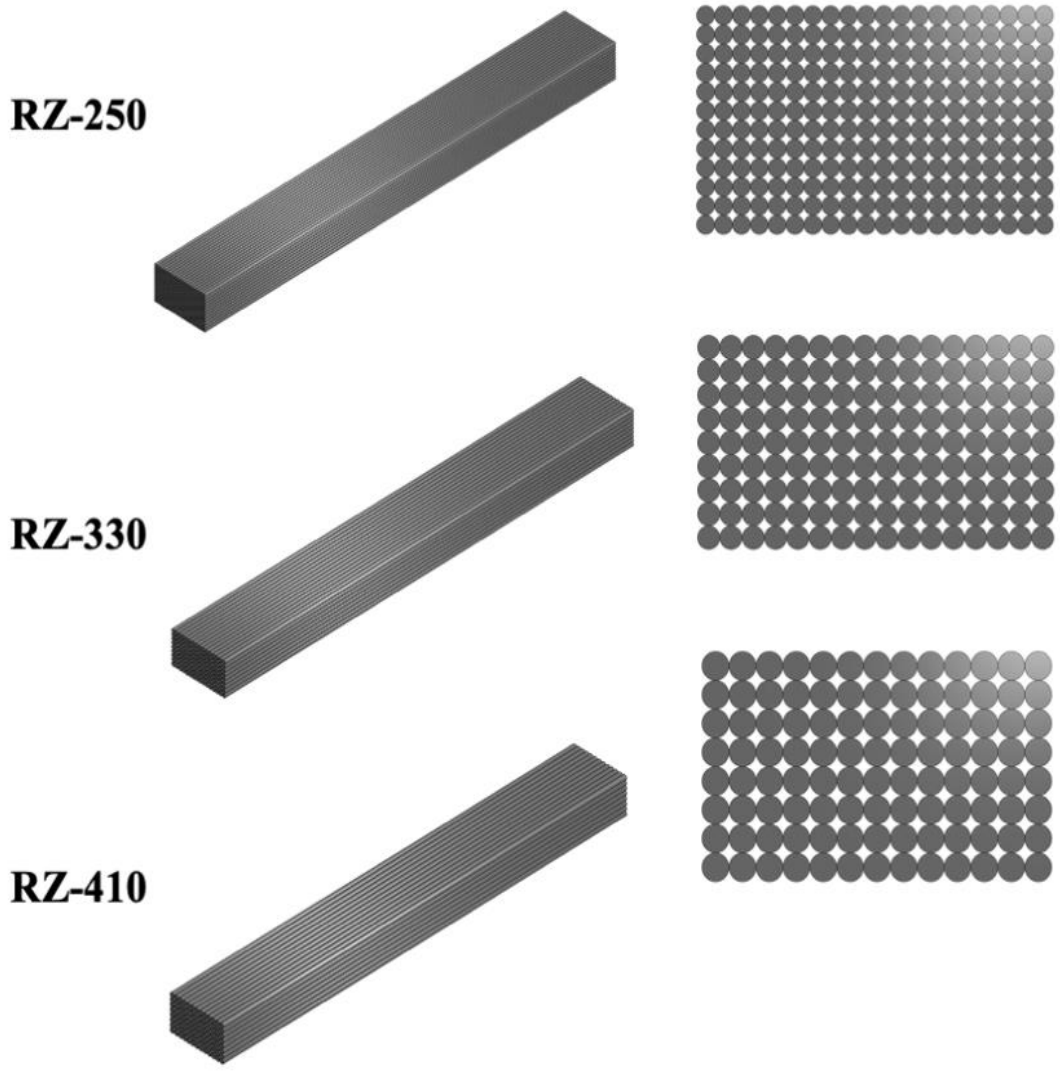

Figure 1 - Schematic representation of the specimens used in the three-point flexural strength tests, highlighting for the transverse cross section as a function of filament diameter. RZ-250, RZ-330 and RZ-410 are the designation of robocast zirconia samples (RZ) printed with extrusion nozzle diameter of 0.25, 0.33 and 0.41 mm (250, 330 and 410 μm), respectively.

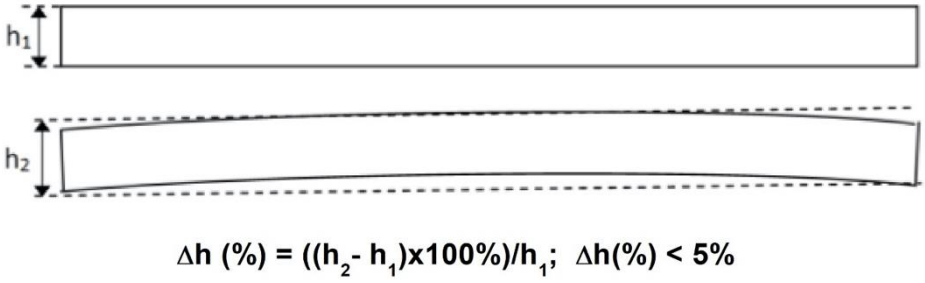

Figura 2. Zirconia (3Y-TZP) green samples obtained by Robocasting with the requirements for the samples to proceed with the sintering step and the three-point flexural strength tests.

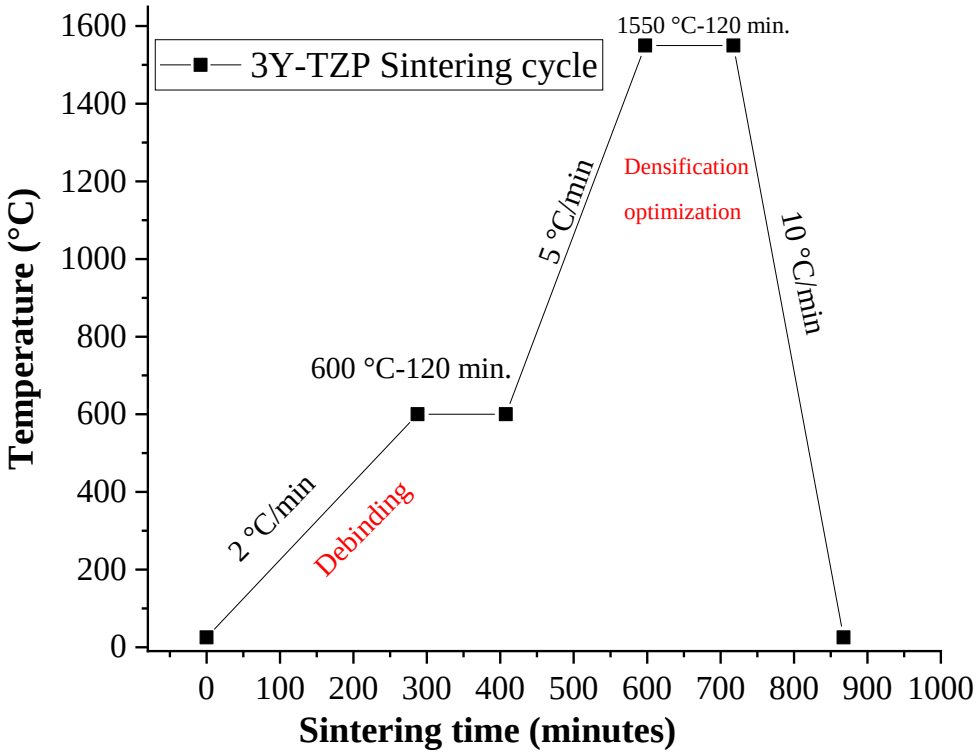

Figure 3. Sintering schedule adopted in this work for 3Y-TZP samples fabricated by robocasting.

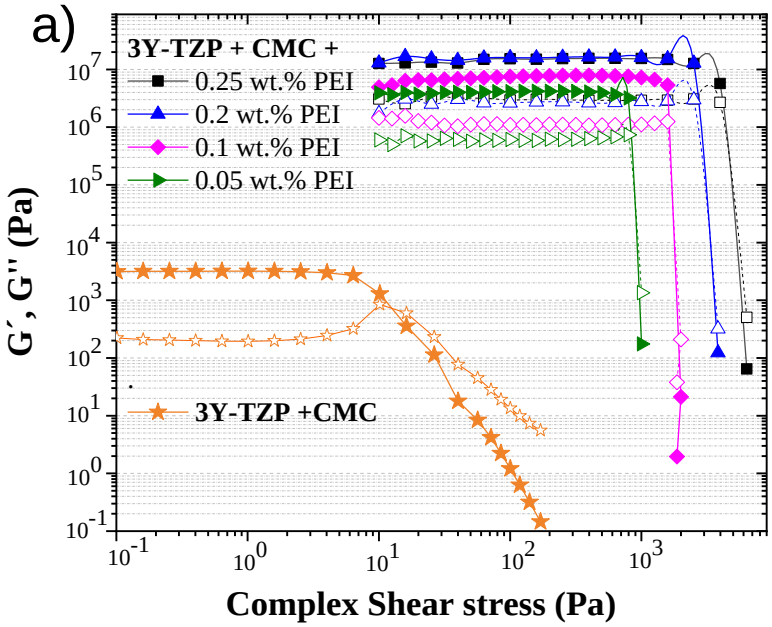
a)
3Y-TZP + CMC +
0.25 wt.% PEI
0.2 wt.% PEI
0.1 wt.% PEI
0.05 wt.% PEI
3Y-TZP +CMC
G´, G'' (Pa)
Complex Shear stress (Pa)

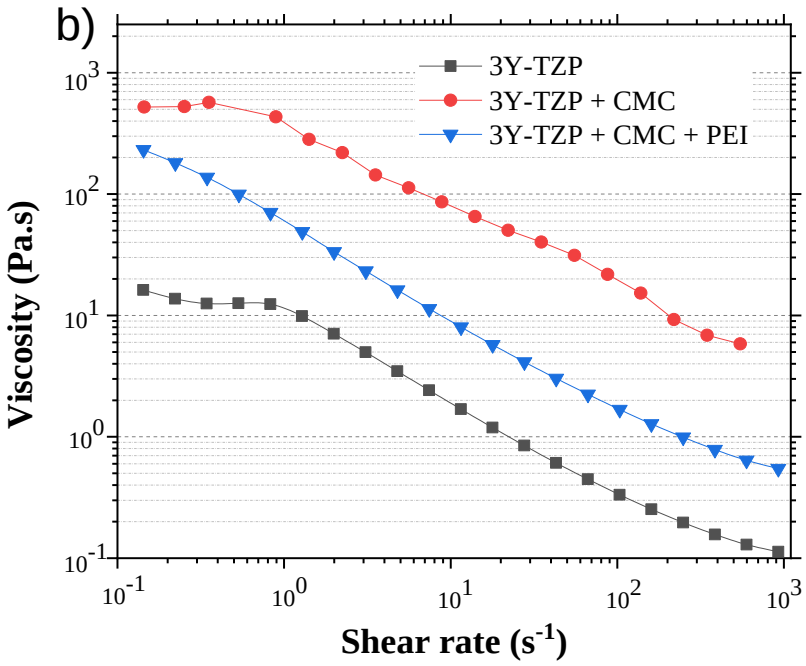

Figure 4. a) Amplitude sweep of 3Y-TZP suspensions (45 vol% of solids) in presence of 0.2 wt% of CMC and different amounts of PEI (0.05, 0.1, 0.2 and 0.25 wt%) as inks, in comparison with the same suspension containing only 0.2 wt% of CMC; full symbols corresponds to G´ (Storage modulus) while open symbols corresponds to G''(Loss modulus); b) Viscosity versus shear rate of suspensions/inks containing 45 vol% of solids: i) without additives (3Y-TZP), ii) in presence of 0.2 wt% CMC (3Y-TZP + CMC) and iii) with 0.2 wt% CMC and 0.2 wt% PEI (3Y-TZP + CMC + PEI).

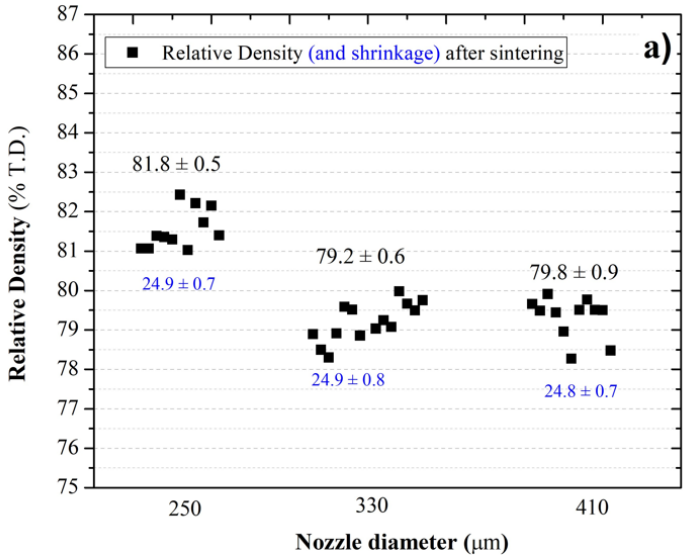

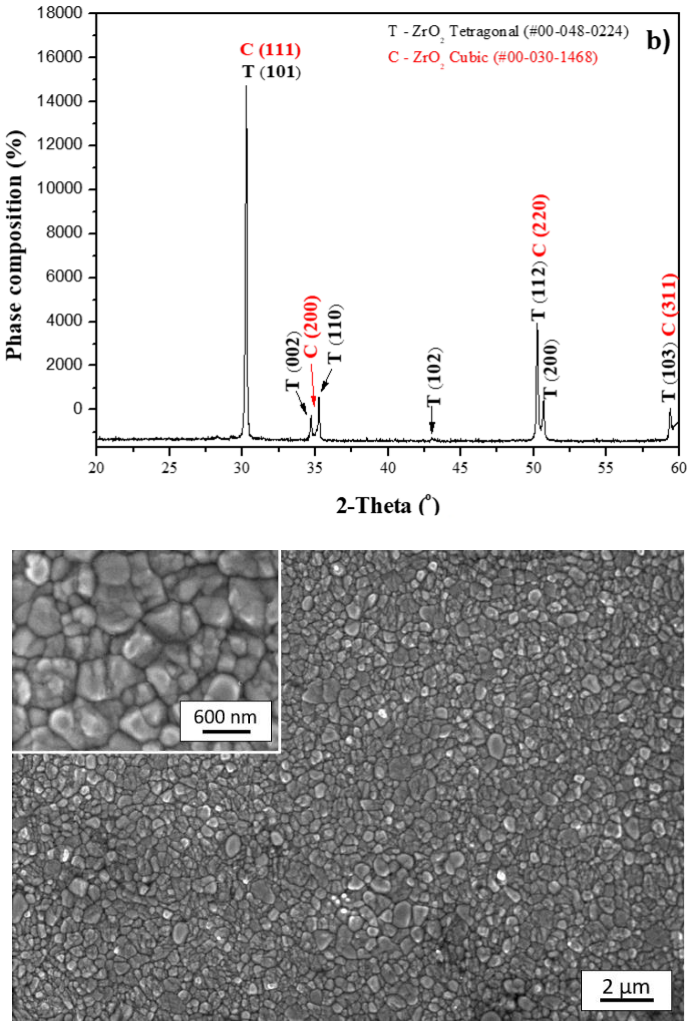

Figure 5. a) Relative density and shrinkage profile of sintered samples as a function of extrusion nozzle diameter; b) typical XRD pattern obtained for the sintered samples; c) SEM micrographs of the sintered 3Y-TZP samples obtained by robocasting.

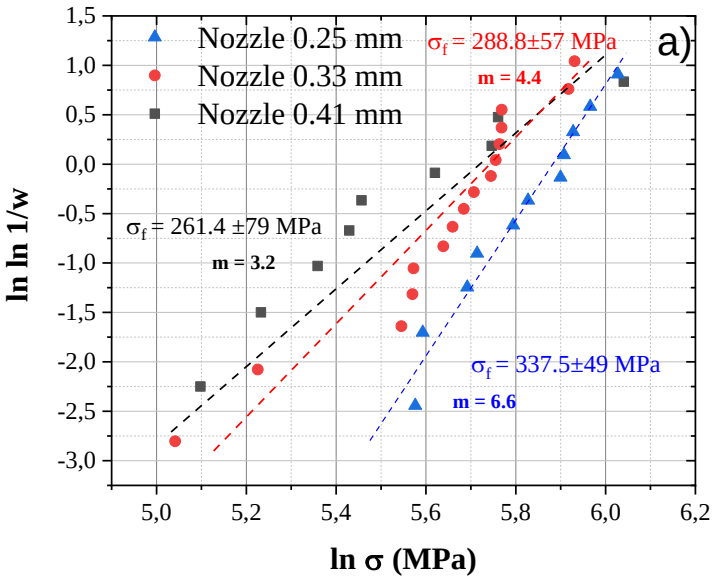

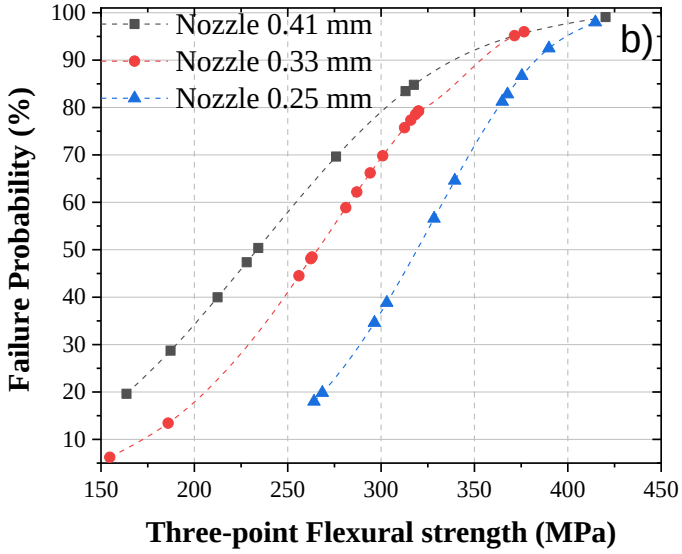

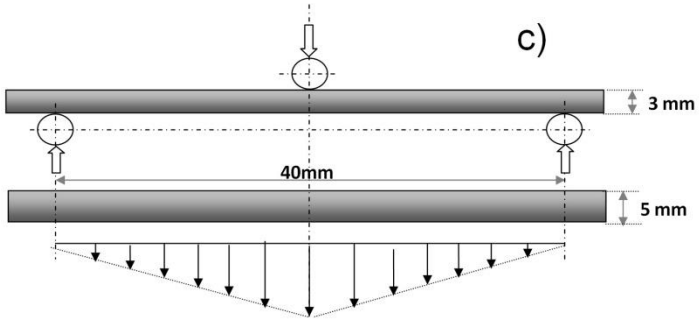

Figure 6. Weibull plot, were: w = 1/(1-pf) (Quinn and Quinn, 2010) **(a)**; failure probability as function of flexural strength of sintered 3Y-TZP samples obtained by Robocasting **(b)** ; schematic profile of three-point flexural testing **(c)**.

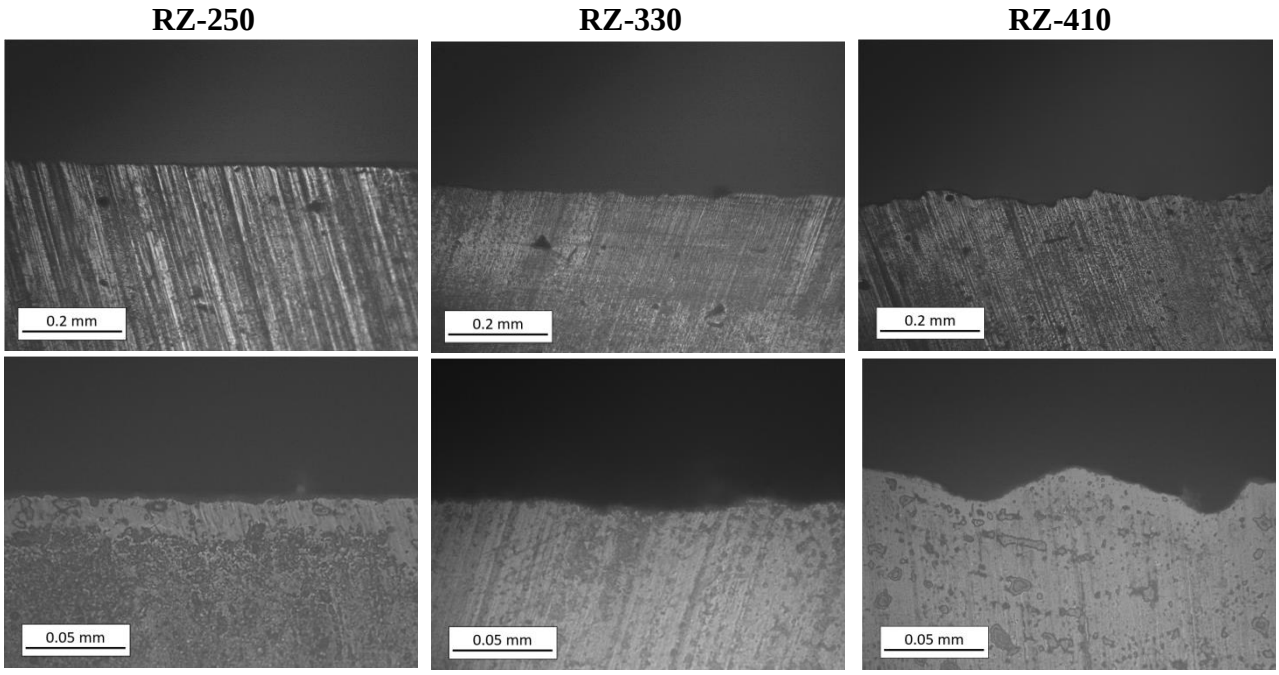

Figure 7. Representative cross sections of 3Y-TZP tensile surfaces submitted to 3-point flexural testing. RZ-250, RZ-330 and RZ-410 are the designation of robocast zirconia samples (RZ) printed with extrusion nozzle diameter of 0.25, 0.33 and 0.41 mm (250, 330 and 410 μm), respectively.

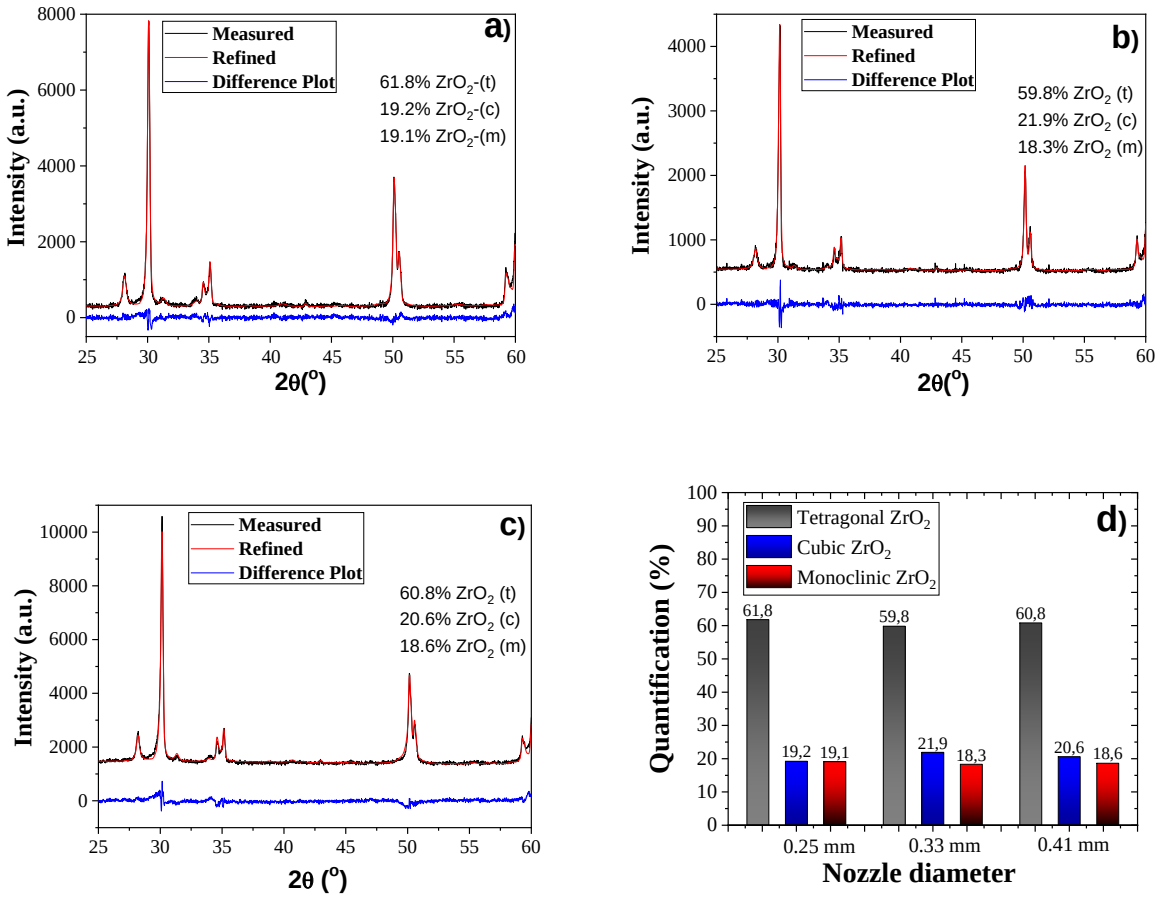

Figura 8. XRD patterns of the fracture surface, after flexural strength tests, of 3Y-TZP sintered samples fabricated by robocasting, for different extrusion nozzle diameters: a) RZ-250; b) RZ-330; c) RZ-410; and d) respective crystalline ZrO_2 phases quantification.

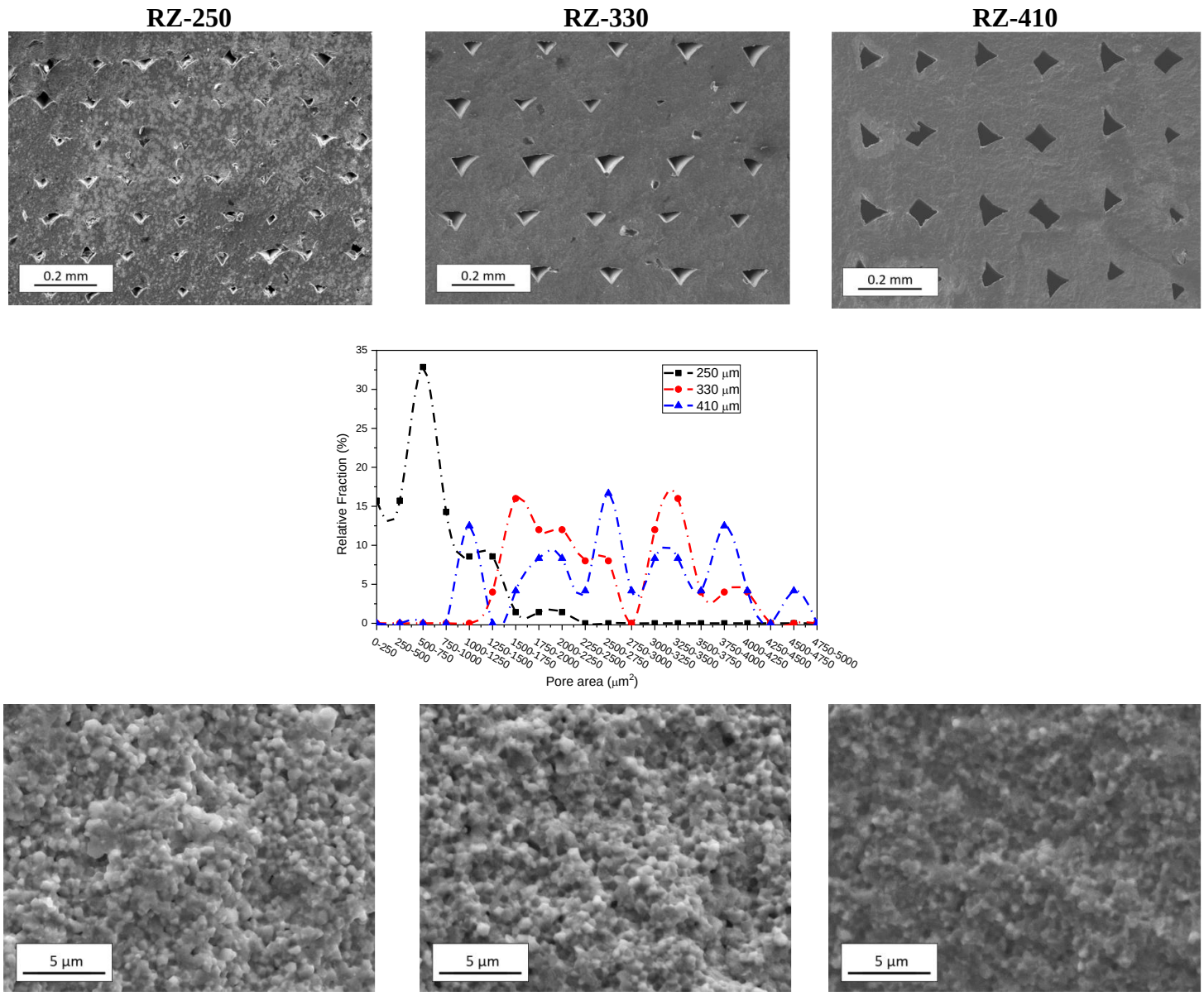

Figure 9. SEM micrographs of fracture surfaces of the 3Y-TZP sintered samples fabricated by robocasting with different extrusion nozzle diameters. The graph presents porosity analysis (relative volume fraction *versus* pore area) from the low amplification images by *ImageJ* software.

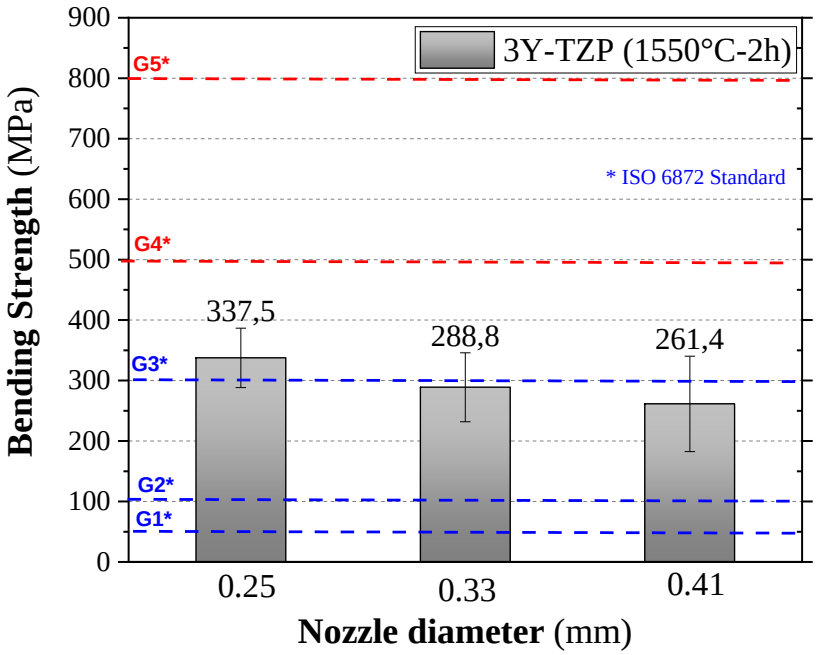

Figure 10. Flexural strength of 3Y-TZP sintered samples fabricated by robocasting front to ISO 6872 recommendations for dental ceramics.

** Group 1: a) Monolithic ceramic for single-unit anterior prostheses, veneers, inlay, or onlays adhesively cemented; b) Ceramic for coverage of a metal framework or a ceramic substructure. Group 2: a) Monolithic ceramic for single-unit anterior or posterior prostheses adhesively cemented; b) Partially or fully covered substructure ceramic for single-unit anterior or posterior prostheses adhesively cemented. Group 3: a) Monolithic ceramic for single-unit anterior or posterior prostheses and for three-unit prostheses not involving molar restoration adhesively or non- adhesively cemented. b) Partially or fully covered substructure for single-unit anterior or posterior prostheses and for three- unit prostheses not involving molar restoration adhesively or non- adhesively cemented. Group 4: a) Monolithic ceramic for three-unit prostheses involving molar restoration; b) Partially or fully covered substructure for three-unit prostheses involving molar restoration. Group 5: Monolithic ceramic for prostheses involving partially or fully covered substructure for four or more units or fully covered substructure for prostheses involving four or more units*